Colloid Polym Sci 280: 218–227 (2002)
© Springer-Verlag 2002

ORIGINAL CONTRIBUTION

Anna Peytcheva
Helmut Cölfen
Heimo Schnablegger
Markus Antonietti

Calcium phosphate colloids with hierarchical structure controlled by polyaspartates

Received: 11 May 2001
Accepted: 14 September 2001

A. Peytcheva · H. Cölfen
M. Antonietti (✉)
Max Planck Institute of Colloids
and Interfaces, Am Mühlenberg 1
14476 Golm, Germany
e-mail: pape@mpikg-golm.mpg.de
Tel.: +49-331-5679501
Fax: +49-331-5679502

H. Schnablegger
Institute of Physical Chemistry
University of Hamburg, Bundesstrasse 45
20146 Hamburg, Germany

Abstract Precipitation of calcium phosphate in a double-jet experiment in the presence of sodium polyaspartic acid results in a structural evolution of stable colloidal objects with a variety of unconventional morphologies. This structural evolution is characterized by a combination of techniques, namely static and dynamic light scattering, small-angle and wide-angle X-ray scattering, and transmission electron microscopy. It is shown that after immediate formation of amorphous precursor nanoparticles with a "parachute architecture", the system transfers into a hollow sphere morphology in the 500-nm region and is composed of plateletlike nanocrystals, and again is transferred into a final, "snowballlike" morphology of high structural definition and monodispersity. The kinetics depends on the amount and the molecular weight of the polymer, but similar structural elements are found in all the cases examined. When repeated in a triple-jet experiment, which also ensures a constant polymer concentration, it was possible to intercept a postulated intermediate structure in practically complete yield, namely crystalline hydroxyapatite nanofibres with extremely high axial ratios which form an interwoven gel.

Keywords Crystallization control · Calcium phosphate · Polyaspartate · Morphosynthesis · Biomineralization

Introduction

Biominerals have proven to be composite materials exhibiting extraordinary behavior regarding their shape, material characteristics, but also stability and adaptability under stress. This is due to the controlled growth of inorganic nanocrystals into an organic matrix which controls the shape and the arrangement of the inorganic building blocks on a hierarchy of length scales. Calcium phosphate is presumably the most important compound in biomineralizing systems. It is found in different modifications depending on the particular system. A high content of hydroxyapatite (HAP) is detected in bones and teeth [l], octacalcium phosphate (OCP) is a precursor phase for HAP in bones/teeth [l] as well as dicalcium phosphate dihydrate (DCPD), also known as brushite, which possibly transforms to HAP via OCP [2]. DCPD is also found in small proportions in urinary [3] and dental stones [4].

There is evidence that the modification of the stabilized calcium phosphate depends on the type and the concentration of proteins participating in the mineralizing process. Mimicking the special growth processes ex vivo may lead to synthetic counterparts which are important for a number of biomedical applications, namely as bone cement [5] or for tooth fillings able to be reconstituted by the body [6].

If one crystallizes a "complicated" system such as calcium phosphate with or without additives, one should be aware of the factors ruling precipitation of the mineral phase from a supersaturated solution without any additives. For calcium phosphate at a given

temperature and pressure the formation of a variety of modifications is possible, mainly depending on the pH as evident from a phase diagram [7].

According to Ostwald's rule of stages, the first phase formed will be a result of the fastest chemical reaction, in many cases amorphous calcium phosphate (ACP). These phases of higher solubility serve as a precursor for the crystallization of less soluble species, finally leading to the (under standard conditions) most stable HAP [7]. Liu and Nancollas et al. [8] suggested a model for the stability of those calcium phosphate phases by considering a number of contributions to the interface energy for the crystal–water system. Especially the surface tensions of the different calcium phosphate phases, which have been interpreted in terms of Lifshitz–van der Waals and Lewis acid–base components [9], showed to be of special importance for the nucleation of various mineral phases [10]. Also, the well-known Ostwald ripening of small crystallites has been interpreted in terms of a net negative interfacial tension between solid and solution [11].

As an example for the phase transition of calcium phosphate, the addition of $CaCl_2$ and Na_2HPO_4 solutions with a Ca/P ratio of 1.67 at ambient pressure and temperature at first gives ACP. If it is left in the solution it is converted within a few hours to DCPD, which is seen as flat plateletlike birefringent crystals in a light microscope. As a stable state is not reached yet, those crystals transform into fine birefringent needles identified as HAP in agreement with the prediction from considerations of the interfacial tensions that DCPD is a precursor for HAP mineralization [10].

The motive of this work was to influence this cascade of processes by adding synthetic polypeptides mimicking the action of natural proteins, both to learn about the mineralization mechanisms as well as to generate new colloidal calcium phosphate/polymer nanostructures. We used poly(sodium)aspartate [(Na-PAsp)] with two different molecular weights as an additive, since the emerging dispersions exhibit long-term stability and in previous studies, it was suggested that PAsp shows site-specific adsorption onto the (100) and (010) faces of OCP, resulting in remarkable selective growth inhibition [12]. It is remarkable that only 1% of PAsp adsorption onto the OCP (100) face area was sufficient to inhibit the OCP growth by 20%, suggesting a dynamic adsorption/desorption equilibrium as found for PAsp adsorption onto the (010) face of DCPD [13]. In the present study, the structure evolution from a nanometer to a micrometer scale is analyzed using a variety of scattering and imaging techniques. Results from small-angle X-ray (SAXS) and static light scattering (SLS) are supported by dynamic light scattering (DLS) and compared with images gained from transmission electron microscopy (TEM) and scanning force microscopy (SFM). Wide-angle X-ray spectroscopy (WAXS) was used to evaluate the type and the amount of the crystal species in the samples.

Experimental

Analytical methods

Light scattering was performed with an ALV 5000 multiple-tau correlator (ALV-Laser, Langen) for simultaneous SLS and DLS experiments. As a light source, a continuous-wave, frequency-doubled Nd-YAG laser (Coherent-Adlas) operating at 532 nm was used. The scattering functions were analyzed using an updated version of the program ORT [14], which transforms SLS curves into pair-distance distribution functions (PDDFs) and takes into full account the parasitic contributions of reflected light from the glass walls of the sample holder. The PDDFs were subsequently interpreted in terms of monodisperse spheres with radial polarizability densities to be determined by the program DECON [15].

SAXS was conducted with a Kratky compact camera equipped with a stepping motor and a counting tube with an impulse height discriminator. The light source was a standard X-ray tube with a fixed copper target operating at 40 mA and 30 kV. The scattering functions were transformed into real-space functions using the ITP program as described by Glatter [16].

TEM images were acquired using a Zeiss EM 912Ω at an acceleration voltage of 120 kV. One droplet of the suspension was applied to a 400 mesh carbon-coated copper grid and left to dry in air. Thermogravimetric analysis (TGA) measurements were performed with a Netzsch TG209 cell. WAXS patterns for identification of the crystalline species were collected using an Enraf Nonius FR590 diffractometer.

Mineralization procedures

For crystallization, a so-called double-jet setup was used where 0.5 M $CaCl_2$ and 0.3 M Na_2HPO_4 solutions were continuously added with a speed of 10 ml/h via thin capillaries to 100 ml 0.1 wt% (variable in subsequent experiments) polymer solution stirred in a reactor [17]. The stoichiometry was chosen for the formation of HAP. The two jets were directed toward each other and this resulted in a very high supersaturation of ions in one spot, thus leading to the immediate formation of calcium phosphate nuclei. These primary nuclei were dispersed in the reactor, brought into contact with the polymer, and growth proceeded according to Ostwald ripening on a much longer timescale up to 1 h region. Previous work [18, 21] shows that this procedure gives rather monodisperse colloids with high structural definition and high reproducibility between the experiments, which is not trivial for crystallization experiments.

The overall concentration of mineral and the ratio of mineral to polymer is controlled by the duration of the jetting procedure. For the precipitation free of additives, the solution becomes immediately turbid with amorphous nuclei. Within 4 h it clears and fine flat crystals are observed. In the presence of Na-PAsp clear solutions are obtained throughout the experiment, hinting at the formation of stable colloidal species.

Thermally polymerized D-L-Na-PAsp with molecular weights of 10,000 and 18,000 $gmol^{-1}$ was donated by Rohm & Haas (Philadelphia) and was used without any further purification. As emphasis is put not only on structure analysis of the samples but also on their dynamics, the previously mentioned experiment was performed using different concentrations of Na-PAsp. The polymer itself was dissolved in doubly deionized water. The measured pH value for all the solutions of 18,000 $gmol^{-1}$ Na-PAsp was 8.1, for solutions of 10,000 $gmol^{-1}$ Na-PAsp it was 6.9, which is due to a different degree of neutralization.

Results and discussion

The relatively slow process of recrystallization from a nanoparticulate precursor state and the colloidal stability in the presence of the polymers enable the structure evolution to be analyzed by various methods. After 1 h of addition, the double-jet process was stopped and the dispersions obtained were filtered with Sartorius filters (Göttingen) with a pore size of 800 nm and introduced to the light scattering setup. As shown in Fig. 1 for the solution of 0.4 wt% 18,000 $gmol^{-1}$ Na-PAsp, the primary particles have a hydrodynamic radius of about 100 nm. This is – more or less – true for all polymer concentrations, i.e., this characterizes the primary precipitation event to presumably amorphous precursor particles generated by the fast precipitation in the double jet and is not due to polymer addition. This size of the primary seed particles for subsequent crystallization is further underlined by the finding of plateletlike calcium phosphate of about the same size in an independent study of HAP precipitation at pH 6.3 [22].

As can be seen in the picture, after a certain "induction time" a pronounced nonlinear growth with time is observed until a plateau is reached after about 70 h. The final size depends on the polymer concentration: here, a radius of 400 nm is found, which does not change over the following weeks. Similar stable regions are found for all Na-PAsp concentrations greater than 0.1 wt%, and the formation of a precipitate is completely suppressed. Less polymer results in unstable colloidal situations. For the determination of the relative composition, the hybrid structures were centrifuged off and then dried. The solid hybrid materials were analyzed by thermogravimetry. The relative loss of weight in percent depending on temperature for various concentrations of the additive is illustrated in Fig. 2.

The weight loss up to about 200 °C is due to adsorbed and crystal-bound water, which is always of the order of 10–20 wt%. The high amount of adsorbed water speaks for the rather high surface areas of these systems. It is remarkable that the pronounced step at 200 °C for the low polymer concentration gets shallower with increasing polymer concentration until it vanishes completely. This effect is due to the swollen polymer layer on the stabilized particles. Whereas at the low polymer concentration, almost exclusively adsorbed and crystal-bound water is released up to 200 °C resulting in a pronounced step in Figure 2, at the higher polymer concentrations, the contribution of the water in the polymer shell which is more easily released becomes more and more pronounced. Hence, an almost continuous transition is observed between water release and polymer decomposition.

A second loss up to 450 °C is due to a transition of HAP leading to a mass loss of 5 wt% which is assumed to be constant for all the samples. The third loss, up to 550 °C, is due to the polymer. In all cases, the structures are mainly inorganic: for a concentration of 0.1% the particles contain 17 wt% water, 1 wt% polymer, and 82 wt% calcium phosphate, whereas the sample made at a polymer concentration of 1% is composed of 12 wt% water, 23 wt% polymer, and 65 wt% mineral. This hybrid composition is similar to tooth enamel: enamel of "old" teeth contains about 1% polymer and 4% water, whereas that of "freshly grown" teeth contains 30% polymer and 38% water.

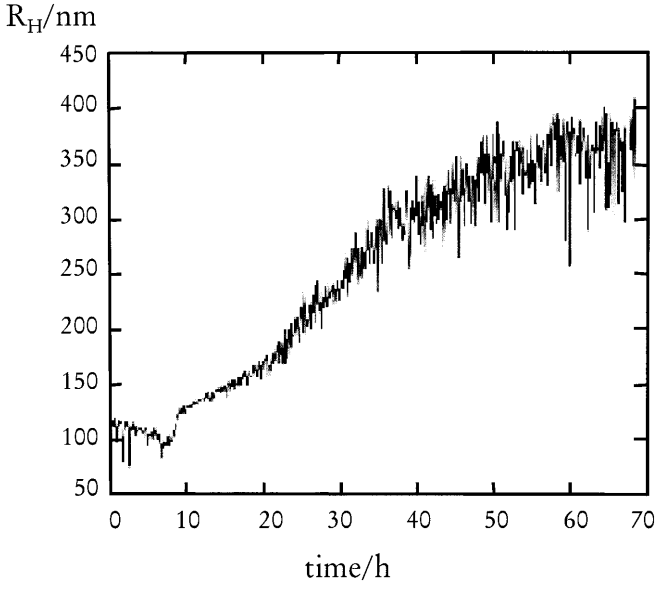

Fig. 1 Dynamics of structural growth of the mineralization reaction, as characterized by dynamic light scattering. R_H is the hydrodynamic radius

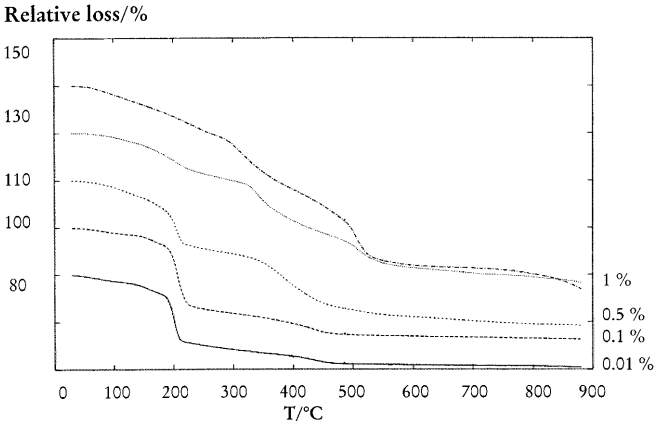

Fig. 2 Thermogravimetric analysis of the resulting hybrid structures, characterizing the amount of bound water and polymer in the hybrids. The first step, at 200 °C, is due to the bound water, whereas mass loss up to 500 °C is due to the polymer

We also tried to characterize the primary structure as obtained directly after the precipitation process, and X-ray diffraction essentially revealed an amorphous material in all cases. From electron microscopy, a rather well defined and interesting core/shell morphology was found (Fig. 3), where the inorganic material formed a compact core surrounded by a "fluffy" shell of PAsp. This structure resembles the "parachute" architecture described by Jung and coworkers [23, 24] for the precipitation of amorphous polymers from vesicle bilayers.

The structural evolution coupled to the growth process characterized in Fig. 1 has to be accompanied by in situ structure analysis in solution. This is done using SLS and SAXS as scattering techniques operative on different length scales.

The SLS scattering curve for all the solutions with a Na-PAsp concentration higher than 0.1 wt% shows the characteristics of developing compact, highly monodisperse systems with sizes in the order of the wavelength of light. Local minima and maxima of the light scattering intensity, $I(q)$, arise faster with increasing polymer concentration.

This structure evolution is demonstrated graphically in Fig. 4, where the development of $I(q)$ within 6 days is shown for the concentration 1 wt.% Na-PAsp with a molecular weight of 18,000 $gmol^{-1}$.

The presence of a defined intermolecular structure can be excluded by considering the values of $I(q)$ at small q values; this means that each growth event occurs independently, but is governed by the same rules. It is also seen by the typical texture of the scattering profile that the structures formed are extremely well defined (monodisperse) and exhibit spherical symmetry, since no less than three oscillations of the structure factor become visible in the q range of light scattering. Decreasing the polymer concentration also decreases the control over the formation of the particles: here, particles with about the same size (about 500 nm), but without visible oscillations of the structure factor are found.

WAXS results on these samples only reveal an unstructured scattering, which might be due either to ACP or to nanocrystallites with dimensions smaller than 10 nm. The results may be interpreted in terms of highly monodisperse associative aggregates composed of smaller mineral units, glued together by the polymer. The attachment of several particles to one polymer chain is well known in flocculation processes and is in accordance with results obtained for similar polymers and $CaCO_3$ [25]. In order to analyze the internal structure of the monodisperse particles obtained, the SLS data were quantitatively evaluated in two steps. At first, the scattering curves were transformed into the corresponding radial PDDF. Special care had to be taken to correct for the reflected light from the sample cell. This antireflection correction is a standard feature of the program ORT (see Experimental). In the second step, the PDDFs were deconvoluted into their corresponding apparent radial polarization density profile, by applying Glatter's DECON program. The numerical stabilities of the two inversion steps turned out to be good, i.e., the assumed spherical symmetry did not cause systematic deviations from the experimental data.

The evolution of the scattering curve of the mineralization reaction in the 0.1 wt% Na-PAsp solution measured over 16 days is shown in Fig. 5a; the corre-

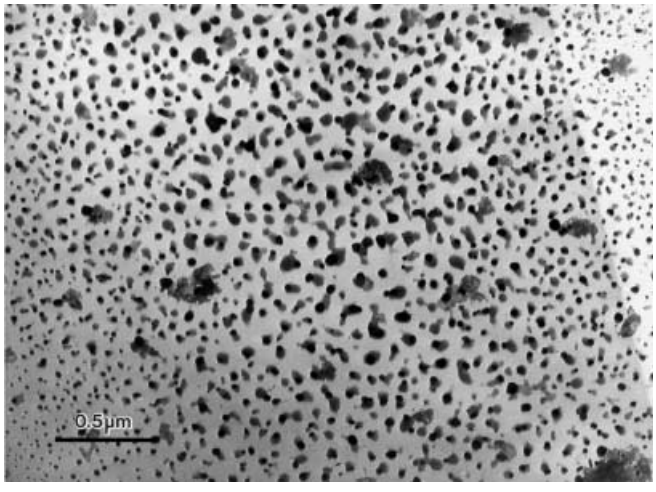

Fig. 3 Transmission electron micrograph of the dried primary structures. Is clearly seen that the polymer forms separated aggregated species 50–100 nm in size. Note that in each of the aggregates there is a spherical, presumably amorphous calcium phosphate particle with higher electron contrast. This is called the "parachute" architecture

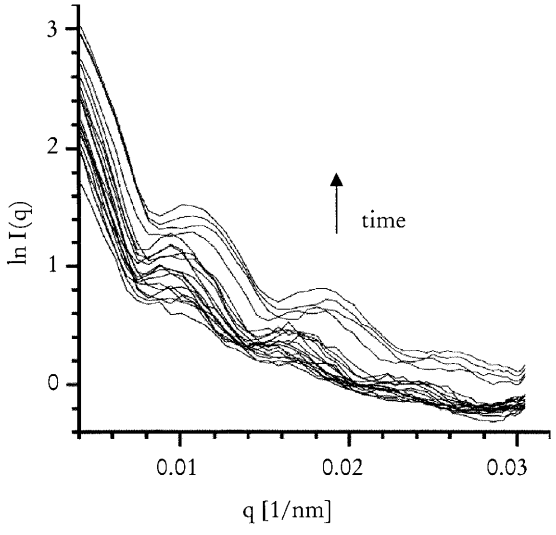

Fig. 4 Structure evolution of the 1 wt% polyaspartate system with time, as characterized by static light scattering. One can clearly observe the development of a spherelike structure factor by its pronounced oscillations, characterizing a well-defined and rather monodisperse system

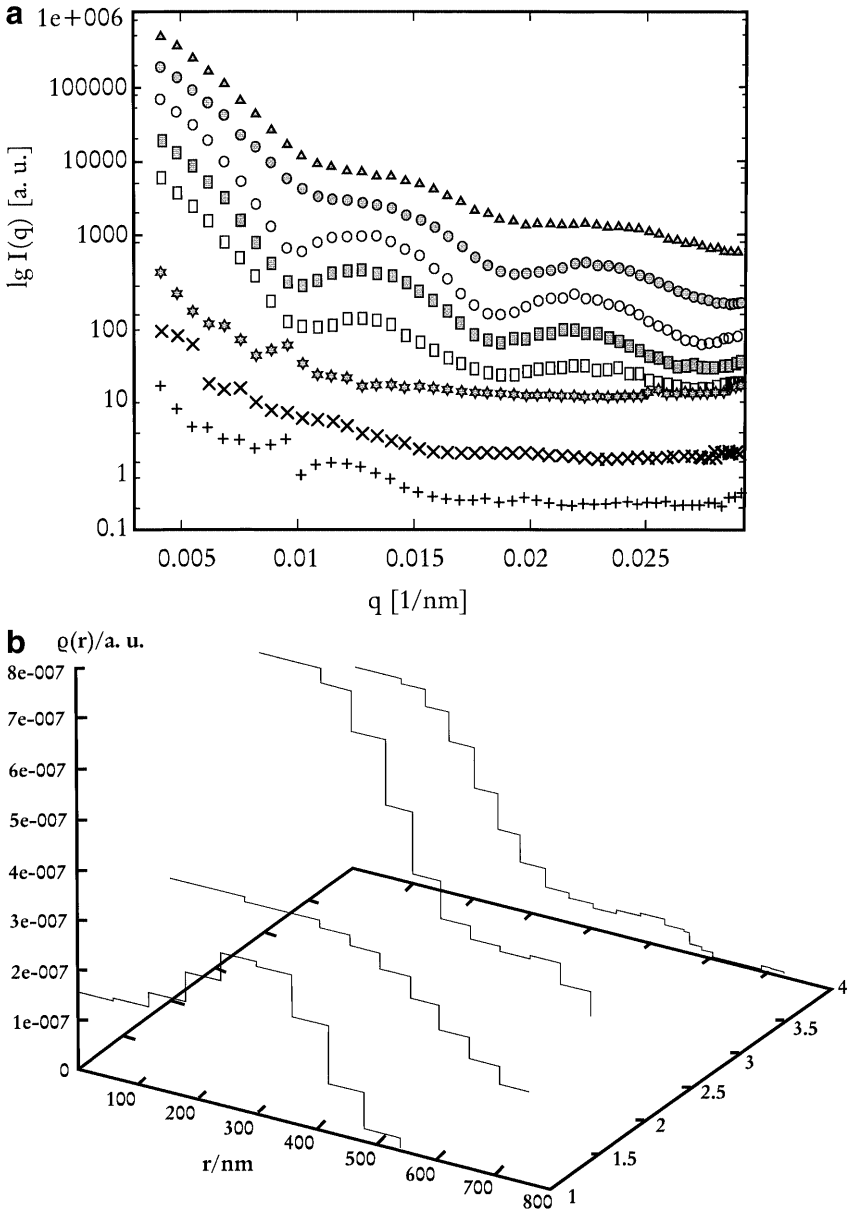

Fig. 5a,b Time-dependent static light scattering of the 0.1 wt% polyaspartate mineralization reaction; the whole set of curves described the evolution over 16 days. **a** Development of the static structure factor in the light scattering region; **b** corresponding radial density functions of spherical aggregates fitted to the structure factor. It is seen that the structures transform from hollow spheres into more compact structures

sponding calculated radial density profiles for four selected times are presented in Fig. 5b.

At the beginning, some type of hollow sphere morphology with a radius of 500 nm and a lower scattering density inside is found. The complete further ripening is described by a rearrangement of this structure, with the final product having the highest density in the middle of the structure, whereas the overall size is more or less constant, i.e., each particle is transformed, but the number of sites essentially stays constant. Such dynamic behavior is hard to reconcile with the classical concept of crystal growth or Ostwald ripening. Also, it differs from the SLS finding that Na-PAsp concentrations above 0.1 wt% yield compact particles.

In contrast to simple crystals, spherical symmetry as well as high monodispersity of superstructures of nanocrystals seem to be rather general features, as described already a number of times in the literature (e.g., Ref. [26]). Nanosize calcium carbonate crystallites have been made using other polymer additives, and small vaterite nanocrystals are associated with monodisperse spheres with a radius of 2 μm, while the polymer acts as a binder [18]. Such a symmetry possesses a minimized interfacial energy and provides the highest colloidal stability.

For the present system, the observed dynamics can be due to free rearrangement of the single compartments or to permeability for ions from the solution. The in situ SAXS measurements, which are sensitive to the struc-

ture of the particles on a length scale below 50 nm, are decisive for the confirmation of one of these scenarios. The SAXS scattering curve for the 1 wt% solution after two different types of sample pretreatment is shown in Fig. 6a as an example.

The lower curve is obtained after filtering the dispersion with a pore size of 200 nm, which should be small enough to remove all the big particles and leave only a potential sol fraction. The scattering signal of a reference measurement of pure water is subtracted from this sample. Fourier transformation of $I(q)$ leads to the pair correlation function, $p(r)$, shown in Fig. 6b. This can be interpreted in terms of cylindrical symmetry with 6-nm diameter and 24-nm length. This means that the smallest unit detected is given by small, elongated nanocrystals of that size.

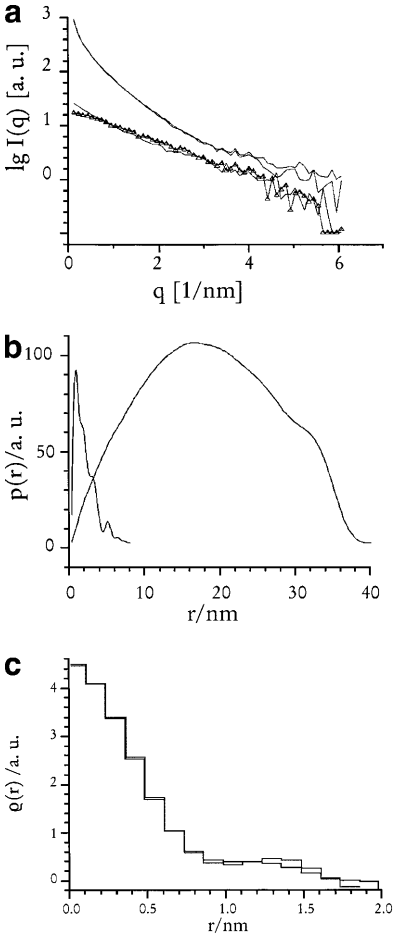

Fig. 6a–c Small-angle X-ray scattering curves of differently treated samples (1 wt% polyaspartate). **a** Sample filtered through a 200-nm (*lower curve*) and a 2-μm filter (*upper curve*); **b** pair correlation functions, as obtained by Fourier transformation of **a**; **c** density distribution along the z-direction of an assumed lamellar structure. One can clearly differentiate between the thin crystalline lamella with high electron density and the adsorbed polymer layer extending another namometer into the aqueous environment

The upper curve in Fig. 6a is obtained after filtering the sample through a 2-μ filter. The signal consequently should consist of the sol fraction and scattering due to the big particles. Subtraction of the sol measurement (lower curve) is expected to give information about the inner architecture of the larger particles.

Since this curve essentially decreases with q^{-2} or as the scattering of a two-dimensional object, a structure model of infinitely extended lamellae with a nonuniform density distribution along the z-axis is applied. As in the given SAXS experiment the scattering vector, q, is restricted to the minimum value of 0.15 nm^{-1}, such a model is appropriate when the primary crystal lamellae are larger than about 40 nm. Deconvolution of $p(r)$ for this model of lamellae produces the density distribution along the z-axis shown in Fig. 6c. r is the distance from the center of the lamella.

Obviously each lamella consists of a 1.4-nm-thick layer of very high density, presumably the inorganic material (such a layered sheet structure correlates with the crystal structure of DCPD as well as with the results confirming DCPD to be a kinetically favored modification to form first from an amorphous precursor), covered on each side with a layer of 1 nm with significantly lower electron density, presumably the flatly adsorbed polymer. This finding is in qualitative agreement with the suggested intercalated DCPD–PAsp structure which resulted from the adsorption of PAsp in the ß-sheet conformation onto the DCPD (010) plane [27].

Mineralization in the presence of the PAsp with lower molecular weight shows a slight variation in the scattering experiments. The superstructures are much smaller, as DLS detects two populations: one with a hydrodynamic radius of 3–4 nm, and the other with a radius of about 120 nm. The SLS curves confirm the presence of particles too small to produce a form factor. The rise in total scattered intensity with time is due to the increasing concentration or size of the scattering units.

The SAXS experiments also reveal the coexistence of two species. Again, before extra filtration, two-dimensional extended structures are identified; after filtration, the remaining can be described as cylindrical in symmetry with characteristic dimensions of 2 nm in diameter and 8 nm in length. Application of the lamellae model to the curve of higher total scattering intensity leads to an identical density distribution as the one obtained for the dispersions of the higher molecular weight Na-PAsp, i.e., the superstructure is composed of polymer-covered single-crystalline sheets.

In contrast to the characterization of the samples in their natural, water-swollen state, the morphology description using TEM only works on dried samples, which both for polyelectrolytes and for calcium phosphate implies a severe change of environment, i.e., we

have to be aware of artifacts. In addition, the fragile calcium phosphate structures are sensitive to the electron beam, so their imaging relies on rather low electron doses.

Clearly, one can observe in Fig. 7a that the first crystalline stages (after 96 h) are characterized by some type of monodisperse, hollow spherical superstructure composed of single crystalline platelets of about 50-nm size. It is noted that the single platelets lie free and well distinguishable around the aggregates. It is speculated that this structure is the conversion of the ''parachutes'' where the previously polymer bound ions and the ACP have recrystallized to platelets onto the surface where the kinetics is fastest. The size increase is explained by a release of the ionic cross-linking sites of the polymer microgel and the coupled swelling.

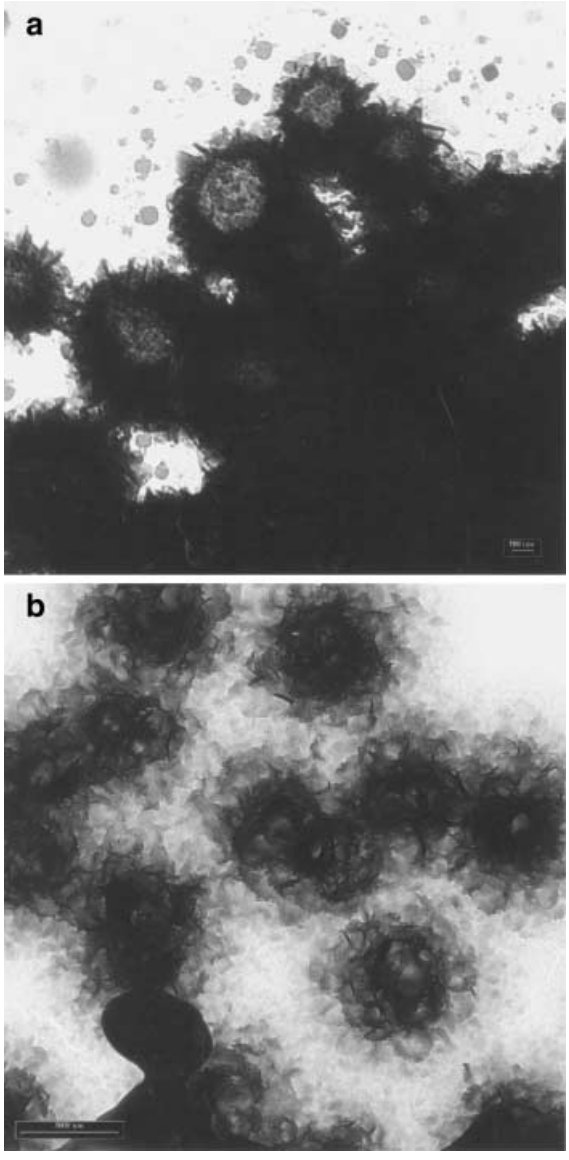

Fig. 7 Transmission electron microscopy of the resulting hybrid structures **a** after 96 h and **b** after 7 days. It is nicely seen that a previously ''hollow-sphere'' structure transfers into a ''snowball-like'' structure

In a rather slow process, this structure transfers to the ''snowball''-like architecture shown in Fig. 7b (after 7 days) where the density of inorganic matter is highest in the inner part. This controlled collapse is due to the mutual attraction of the single plates, which is improved in the final morphology. Owing to the fact that the architectures found in the dried state go very well with the scattering characterization in solution, we can exclude the presence of drying artifacts. It is pointed out that similar ''snowball'' crystal superstructures were already described by Jones et al. for the controlled crystallization of Co_2O_3 in the presence of κ-carrageenan [28].

The isolated, free platelets were characterized with SFM (pictures not shown). They possess mostly a rectangular, triangular, or truncated hexagonal shape with diameters of 50–100 nm and a height (thickness) of about 2 nm. In addition, larger amounts of very thin, boardlike structures with a height of 2 nm, a width of 15 nm, and a length of 50 nm are found, covering most of the mica surface. This again confirms the observations of the X-ray scattering experiments, where size-selective filtering has shown the coexistence of thin platelets (1.4-nm inorganic material plus polymer monolayer) and little rods.

It is possible that the rods or boards are a precursor to the platelets, since thickness and length coincide. To clarify the somewhat unexpected occurrence of these nanorods and to test the question if they are indeed an early stage of polymer-controlled crystallization, we performed a so-called triple-jet experiment. It is an inherent property of the double-jet experiment that it is a controlled, but still heterogeneous, process with respect to the fact that at the beginning of the addition, the ratio of polymer to mineral is very high, whereas just at the end of jetting, the desired relative concentration of polymer to mineral is reached. Since the polymers employed are acids, such a procedure is not suited to isolate fragile precursor structures, and reproducibility is only obtained when polymer adsorption/desorption is fast (compared to the addition) or crystallization is slow (major steps of structure formation take place after completing the addition).

This is why a triple jet experiment was performed where a 0,l w% Na-PAsp solution is added via a third jet to compensate the loss of PAsp throughout the process due to the precipitation in the hybrid particles. The relative ratio of mass fluxes is calculated biom the relative composition of the isolated particles as determined by TGA. By that way, one can ensure the composition of the system to stay always very close to the starting situation.

The TEM analysis of the precipitate and the clear solution formed is presented in Fig. 8. It is seen that the majority of the sample indeed consists of very thin, needlelike calcium phosphate crystals (beside some rarely occurring platelets). These are presumably best seen in the analysis of the sol fraction (Fig. 8a). Again, the tanglelike particles aggregate to spherical clusters with a lower mineral density in the core (Fig. 8b), presumably because of the polymer, which forms microgels owing to the added ions and nuclei. This structural reconstruction is very similar to the transition from hollow spherical superstructures to snowballs already found in the double-jet experiment. Electron diffraction for analysis of the crystallinity of those tangles fails as they are unstable after being exposed to the focused electron beam.

WAXS was performed on the centrifuged and dried sample, and the results are shown in Fig. 9. Starting from the left side, the first two peaks are indicative for the brushite structure, presumably coming from the rare platelets seen in TEM. The third peak can be attributed to a HAP component assigning the (002) crystallographic axis. This would correlate with crystal growth along the *c*-axis of HAP. From the width of the reflex, a correlation length of a crystalline order much smaller than the visible extension of the needles in the micrometer range can be calculated.

This refractogram, however, is not sufficient to decide if the needles are indeed in the HAP phase, since objects largely extended in only one direction possess only a small total number of scattering peaks. The $P_6 3$ symmetry of HAP, however, would favor the growth of thin needles along the *c*-axis. Furthermore, when aligned to the 001 basal face and viewed along the *c*-axis, HAP only exposes the Ca^{2+} cations but not the PO_4^{3-} anions at all faces except (001) (Fig. 10), so a needlelike structure is already favored by adsorption of the polyanionic PAsp to all faces exhibiting positive charges. HAP filament or needle formation was indeed found by selective adsorption of polymers with carboxylate [16] or phosphate groups [29].

If the dispersion is aged in the solution for a few hours, the tangles become shorter and the clusters become more compact (Fig. 8c). This means that the tangles are actively reconstructed, but become shorter and higher in number. Neither the typical result of Ostwald ripening (crystal growth) or of the Ostwald step rule (crystal transformation) are obtained, underlining

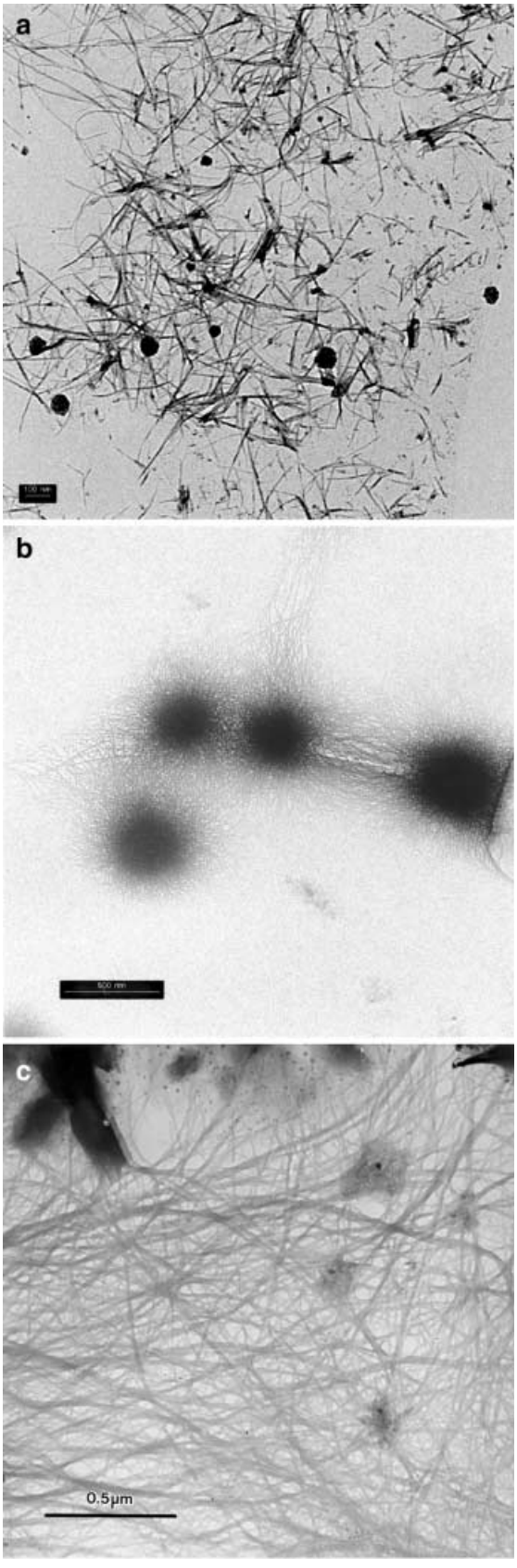

►

Fig. 8a–c Transmission electron microscopy pictures of the result of the triple-jet experiment. **a** Analysis of the sol fraction with its typical nanofiber structure; **b** these fibers aggregate to narrowly distributed, spherical superstructures of about 500-nm diameter; **c** between the particles or locations with higher mineral density, the fibers can form extended nets of high structural definition

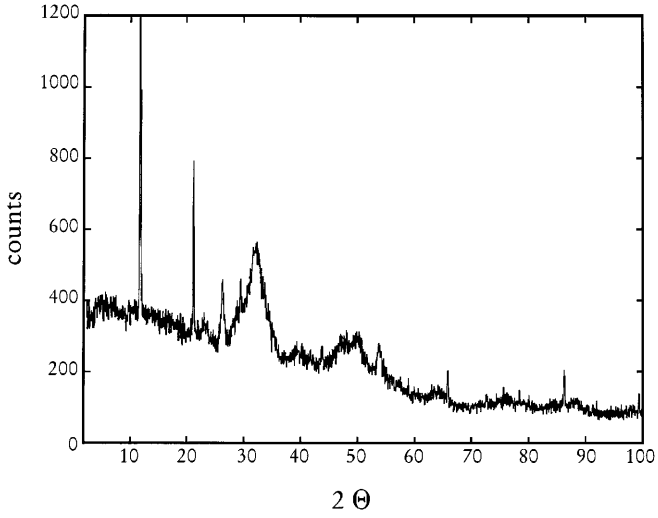

Fig. 9 Wide-angle X-ray scattering diffractogram of the isolated fiber phase

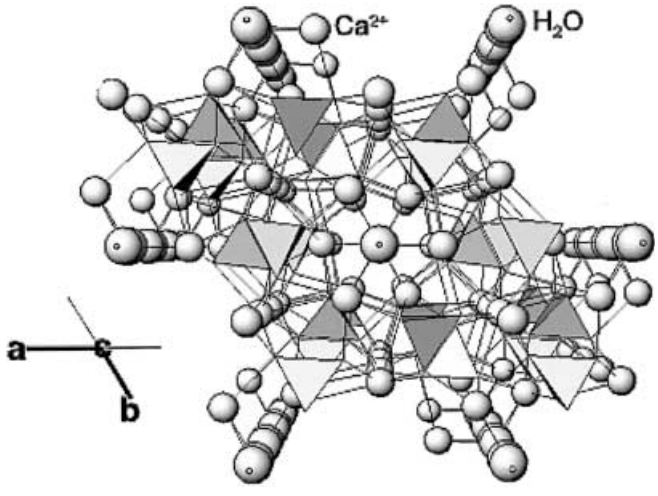

Fig. 10 Hydroxyapatite crystal structure calculated with the WINATOMS software, aligned to the 001 base face so that the view is along the crystal *c*-axis. The *polyhedra* represent the phosphate ions, the *very small spheres* hydrogen, the *intermediate-sized spheres* calcium, and the *larger spheres* oxygen. It is seen that in this fiber orientation, just water and calcium ions are exposed, where the polyanionic polymer can easily bind

the importance of interface energy contributions (triggered by polymer adsorption) for crystalline nanostructures as already suggested by Wu and Nancollas [11].

These observations confirm earlier experiments where very similar tangles were found during the mineralization of calcium phosphate in the presence of a rather complicated micelle-forming, alkylated poly(ethylene)–*b*–poly(methacrylic acid)–C_{12} block copolymer [16]. The present results indicate that needle formation is rather a generic feature of the calcium phosphate system and does not rely on a specific polymer.

Conclusions

Precipitation of calcium phosphate in the presence of a synthetic polypeptide, thermally polymerized poly(sodium-D-L-aspartate) at pH 8.1 results in the formation of a whole cascade of well-defined organic–inorganic superstructures, which were characterized in situ by the combination of a number of techniques.

As a first step, the high supersaturation of calcium and phosphate ions leads to the immediate formation of a polymer-stabilized ACP phase with globular shape or "parachute" architecture and a radius of about 100 nm. Interestingly enough, no flocculate is formed (as Ca^{2+} does for a whole range of polyelectrolytes), but a stable colloidal species is obtained where the PAsp chains are cross-linked by ACP clusters or nanoparticles toward some well-defined microgel. This is the molecular base for scale inhibition or preservation of high supersaturation levels in biological systems, i.e., the calcium phosphate is kept as an amorphous, readily accessible intermediate.

After this stage, very slow recrystallization on the timescale of 70–100 h takes place here most of the new nuclei are still bound to the previous microgel structure, which is presumably due to a combination of kinetic (the very high supersaturation ratios being available in the microgel) and thermodynamic effects (the presence of the aspartate lowers interface energies and increases the probability of nucleation). As a result, first a kinetic structure, a "hollow snowball" composed of single crystal platelets, is formed, which later transforms into a "compact snowball", where the maximal density is in the middle of the particles.

X-ray scattering suggests the simultaneous presence of very tiny calcium phosphate boards or fibrils, a structure which again seems to be a kinetic intermediate; these boards are also not bound to the microgel particles and can be filtered off. Interestingly, the size of these fibrils depends on the molecular weight of the PAsp employed for mineralization. SAXS and AFM reveal 6×24-nm sized sheetlike objects for $M_{\mathrm{pasp}} = 18{,}000$ gmol^{-1}, whereas the lower molecular weight ($M_{\mathrm{pasp}} = 10{,}000$ gmol^{-1}) gives structures with dimensions of 2 nm $\times$ 18.8 nm. This observation is hard to explain by a pattern template mechanism ("epitaxy") or by growth along a helix, an interpretation which was raised for the growth of $BaSO_4$ needles in PAsp solutions [30].

In context with previous observations that the polymers are just temporarily bound and cover just a minority of the platelet surface [8], we attribute this influence to the kinetics of exchange and the coupled growth/dissolution modes which seriously depend on molecular weight [see Ref. [9]; in a simple adsorption model, the detention period varies with $\exp M$]. We rate these observations as a clear hint that structural control

in those systems is not due to some type of epitaxial match between the polymer gel and the induced crystals, but is due to the influence of the polymer on interface energies and growth rates via reversible adsorption equilibria. A comparative discussion between the ''kinetic'' and the ''steoreochemical'' picture was given by Addadi et al. [31].

On the basis of these observations, it was possible to design a ''triple-jet'' experiment, where the conditions of board or fibril formation were kept throughout the addition process. This technique is close to the ''constant composition method'' introduced by Nancollas and Wu [10]. In this case, a practically pure nanofiber morphology could be obtained, where the cross-section of the fibers was of the order of some crystal units cells. We were, however, not able to give an unequivocal proof that these fibers were indeed crystalline, owing to the sensitivity of calcium phosphate phases. The fibrils formed at the beginning had lengths up to the micrometer range, but became shorter and nested with increasing waiting time. This also speaks for the fact that those nanostructures are kinetic objects, i.e., their formation and disappearance is not due to some epitaxial pattern recognition.

Acknowledgement We thank C. Briel for some open discussions. Financial support by the Max Planck Society is gratefully acknowledged.

References

1. Mann S (1996) In: Mann S (ed) Biomimetic materials chemistry. VCH, Weinheim, pp 1–40
2. Mathews JL, Arnott HJ, Brown WE, Dosch W, Hascal VC, Hautmann R, Krampitz GP, Münzenberg KJ, Pritzker KPH, Prockop DJ, Schenk RK, Watabe N, Young RA (1982) In: Nancollas GH (ed) Biological mineralization and demineralization. Springer, Berlin Heidelberg New York, p 345
3. Daudon M, Donsimoni R, Hennequin C, Fellahi S, Le Moel G, Paris M, Troupel S, LacourB (1995) Urol Res 23:319
4. Werness PG, Bergert JH, Smith LH (1982) J Cryst Growth 53:166
5. Yaylaoglu MB, Korkusuz P, Ors UJ, Korkusuz F, Hasirci V (1999) Biomaterials 20:711–719
6. Skrtic D, Hailer AW, Takagi S, Antonucci JM, Eanes ED (1996) J Dent Res 75:1679-1686
7. Nancollas GH (1989) In: Mann S, Webb G, Williams RJP (eds) Biomineralization. Chemical and biochemical perspectives, VCH, Weinheim, p 157
8. Liu Y, Nancollas GH (1997) J Phys Chem B 101:3464–3468
9. Wu WS, Nancollas GH (1998) Pure Appl Chem 70:1867–1872
10. Nancollas GH, Wu WJ (2000) J Cryst Growth 211:137–142
11. Wu WJ, Nancollas GH (1998) J Solution Chem 27:521–531
12. Burke EM, Guo Y, Colon L, Rahima M, Veis A, Nancollas GH (2000) Colloids Surf B 17:49–57
13. Peytcheva A, Antonietti M (2001) Angew Chem Int Ed Engl 40:3380–3383
14. Schablegger H, Glatter O (1993) J Colloid Interface Sci 158:228–242
15. Glatter O (1981) J Appl Crystallogr 14:101–108
16. (a) Glatter O (1977) J Appl Crystallogr 10:415–421; (b) Glatter O (1979) J Appl Crystallogr 12:166–175; (c) Glatter O (1989) J Appl Crystallogr 13:577–584
17. Sedlak M, Antonietti M, Cölfen H (1998) Macromol Chem Phys 199:247–254
18. Cölfen H, Antonietti M (1998) Langmuir 14:582–589
19. Qi L, Cölfen H, Antonietti M (2000) Angew Chem Int Ed Engl 39:604–607
20. Qi L, Cölfen H, Antonietti M (2000) Chem Mater 12:2392–2403
21. Cölfen H, Qi L (2001) Chem Eur J 7:106–116
22. Antonietti M, Breulmann M, Göltner C, Cölfen H, Wong KKW, Walsh D, Mann S (1998) Chem Eur J 4:2493–2500
23. Jung M, Hubert DHW, Bomans PHH, Frederik P, Van Herk A, German AL (2000) Adv Mater 12:210–214
24. Jung M, Hubert DHW, Van Veldhoven E, Frederik P, Van Herk A, German AL (2000) Langmuir 16:3165–3174
25. Rieger J, Hädicke E, Rau IU, Boeckh D (1997) Tenside Surfactants Deterg 34:430
26. Matijevic E (1993) Chem Mater 5:412
27. Sikiric M, Babic-Ivancic V, Milat O, Sarig S, Füredi-Milhofer H (2000) Langmuir 16:9261
28. Jones F, Cölfen H, Antonietti M (2000) Biomacromolecules 1:556–563
29. Rudloff J (2001) PhD thesis. University of Potsdam
30. Benton WJ, Collins IR, Grimsey IM, Parkinson GM, Rodger SA (1993) Faraday Discuss 95:281
31. Addadi L, Moradian-Oldak J, Weiner S (1991) In: Sykes SC, Wheeler AP (eds) Surface reactive peptides and polymers. ACS symposium series 444. American Chemical Society, Washington, DC, p 13